

Modelling the dynamical evolution of the Bootes dwarf spheroidal galaxy

M. Fellhauer¹*, M.I. Wilkinson², N.W. Evans¹, V. Belokurov¹, M.J. Irwin¹,
G. Gilmore¹, D.B. Zucker¹, J.T. Kleya³

¹ *Institute of Astronomy, University of Cambridge, Madingley Road, Cambridge CB3 0HA, UK*

² *Dept. of Physics and Astronomy, University of Leicester, University Road, Leicester LE1 7RH, UK*

³ *Institute for Astronomy, 2680 Woodlawn Drive, Honolulu, HI, 96822, USA*

9 February 2022

ABSTRACT

We investigate a wide range of possible evolutionary histories for the recently discovered Bootes dwarf spheroidal galaxy, a Milky Way satellite. By means of N -body simulations we follow the evolution of possible progenitor galaxies of Bootes for a variety of orbits in the gravitational potential of the Milky Way. The progenitors considered cover the range from dark-matter-free star clusters to massive, dark-matter dominated outcomes of cosmological simulations. For each type of progenitor and orbit we compare the observable properties of the remnant after 10 Gyr with those of Bootes observed today. Our study suggests that the progenitor of Bootes must have been, and remains now, dark matter dominated. In general our models are unable to reproduce the observed high velocity dispersion in Bootes without dark matter. Our models do not support time-dependent tidal effects as a mechanism able to inflate significantly the internal velocity dispersion. As none of our initially spherical models is able to reproduce the elongation of Bootes, our results suggest that the progenitor of Bootes may have had some intrinsic flattening. Although the focus of the present paper is the Bootes dwarf spheroidal, these models may be of general relevance to understanding the structure, stability and dark matter content of all dwarf spheroidal galaxies.

Key words: galaxies: dwarfs — galaxies: individual: Bootes — galaxies: kinematics and dynamics — galaxies: evolution — methods: N -body simulations

1 INTRODUCTION

The dwarf satellite galaxies of the Milky Way have attracted considerable interest in recent years due to their high apparent mass to light ratios, which suggest the presence of considerable quantities of dark matter (DM: Aaronson 1983; Mateo 1998; Kleya et al. 2001). Given the apparent absence of dynamically significant DM in globular star clusters, the dwarf spheroidal galaxies (dSphs) are particularly valuable for DM studies as they are the smallest stellar systems known to contain DM (Gilmore et al. 2007). N -body simulations of galaxy formation in a Λ CDM cosmology predict that a galaxy like the Milky Way should be surrounded by several hundred low-mass satellite halos (e.g. Moore et al. 1999). The small number of known dSphs in the vicinity of the Milky Way has often been cited as a problem for Λ CDM and many attempts have been presented in the literature to explain why the numbers of satellites which formed stars might be much lower than the total number of substructures.

The past two years have witnessed the discovery of a plethora

of new low-luminosity Milky Way satellites (Willman et al. 2005; Belokurov et al. 2006; Zucker et al. 2006; Belokurov et al. 2007; Walsh et al. 2007). These objects probe a previously unexplored regime for galaxies, extending the faint end of the galaxy luminosity function by almost four magnitudes. As Gilmore et al. (2007) discuss, these new objects also extend to fainter magnitudes the apparent bi-modality in the size distribution of low-luminosity stellar systems, with dSphs exhibiting core radii which are always more than a factor of four larger than the half-light radii of the most extended star clusters. Given that all the dSphs brighter than $M_V = -8$ show evidence of DM, while star clusters appear to be purely stellar systems, understanding the physical origin of this size difference may have implications for our knowledge of DM. It is therefore of particular importance to determine whether or not the newly discovered satellites display evidence of DM. The goal of this paper is to investigate whether the current observational data for one of these newly identified satellites can be used to constrain its DM content.

Belokurov et al. (2006) reported the discovery of a faint dwarf galaxy in the constellation of Bootes. The object was discovered during a systematic search for over-densities of stars in the magni-

* Email: madf@ast.cam.ac.uk, nwe@ast.cam.ac.uk, vasily@ast.cam.ac.uk

tude range $16 \leq r \leq 22$ in the Sloan Digital Sky Survey (SDSS York et al. 2000). The morphology of the stellar iso-density contours based on the SDSS data suggested that the system was quite irregular with some hints of the presence of internal substructure, possibly indicating that the object was in the process of tidal disruption. The aim of this paper is to test this hypothesis and constrain the properties of potential progenitors of this system.

The investigation of the evolution of the dSph galaxies around the Milky Way by means of N -body simulations has a long history. Many authors (e.g. Johnston, Sigurdsson & Hernquist 1999; Johnston, Choi & Guhathakurta 2002; Mayer et al. 2002; Read et al. 2006) try to model the initial cosmological halos with or without the luminous component inside, follow their evolution and compare the final results with the population of dSph galaxies of the Milky Way. Mostly these studies focused on the more luminous dwarfs, which were the only known satellites prior to the recent discoveries. In this paper we follow a different approach. We use N -body simulations to investigate the evolution of possible progenitors of Bootes (henceforth Boo). Our goal is to understand the present-day properties of Boo and to determine whether these can be used to constrain the DM content of this satellite and of its progenitor. In § 2 we describe the observed properties of Boo. § 3 summarises the initial conditions for our models. § 4 presents the results of our simulations for a range of possible progenitors and Galactocentric orbits. Finally, in § 5 we assess the relative merits of the various models and describe the follow-up observations which are required to distinguish between them.

2 OBSERVED PROPERTIES OF BOO

The Bootes dSph is currently located at (Belokurov et al. 2006; Siegel 2006)

$$\text{RA} = 14^{\text{h}} 00^{\text{m}} 06^{\text{s}} \quad (1)$$

$$\text{Dec} = +14^{\circ} 30' 00'' \quad (2)$$

$$D_{\odot} = 62 \pm 3 \text{ kpc} \quad (3)$$

After correcting for unresolved and faint stars, Belokurov et al. (2006) calculated that the total luminosity of Boo is $M_{V,\text{tot}} = -5.8$ mag. Taking a conservative stellar mass-to-light ratio of $M/L = 2$ this translates into a total luminous mass of $3.7 \times 10^4 M_{\odot}$.

Muñoz et al. (2006) estimated the bulk radial velocity and line of sight velocity dispersion of Boo to be

$$v_{\text{rad},\odot} = +95.6 \pm 3.4 \text{ km s}^{-1} \quad (4)$$

$$\sigma_{\text{los}} = 6.6 \pm 2.3 \text{ km s}^{-1} \quad (5)$$

based on a sample of seven stars. More recently, Martin et al. (2007) obtained a sample of 30 Boo members and estimated these parameters to be

$$v_{\text{rad},\odot} = +99.9 \pm 2.1 \text{ km s}^{-1} \quad (6)$$

$$\sigma_{\text{los}} = 6.5_{-1.4}^{+2.0} \text{ km s}^{-1} \quad (7)$$

in good agreement with the earlier value. At present no proper motion determination for Boo is available.

Belokurov et al. (2006) compared the colour-magnitude diagram of Boo with that of the old, metal-poor ($[\text{Fe}/\text{H}] \sim -2.3$) globular cluster M92 and concluded that Boo is dominated by a stellar population similar to that of M92, although slightly younger and more metal poor. No evidence of young or intermediate age populations in Boo has yet been found and no traces of HI gas

have been detected (Bailin & Ford 2007). Based on the equivalent widths of the Mg lines in the spectra of their seven Boo members, Muñoz et al. (2006) estimated the metallicity of the system to be $[\text{Fe}/\text{H}] \approx -2.5$, which would make Boo the most metal-poor Milky Way dwarf spheroidal discovered to date. Martin et al. (2007) found a somewhat higher metallicity of $[\text{Fe}/\text{H}] \approx -2.1$ based on the equivalent widths of the CaII near-infrared triplet (CaT) lines from a larger sample of 19 stars. The origin of the discrepancy between these two measurements is unclear, but could be related to the difference in the calibration of the empirical estimators for $[\text{Fe}/\text{H}]$ from the Mg and Ca line-widths. Prior to the work of Battaglia et al. 2007, neither of these measures was calibrated below $[\text{Fe}/\text{H}] \sim -2$ (Rutledge et al. 1997; see also the discussion in Koch et al. 2007). Battaglia et al. 2007 compared abundances derived from high resolution spectra with abundances for the same stars derived from low resolution spectra of the CaT and showed that, although the CaT calibration holds until at least $[\text{Fe}/\text{H}] = -2.5$, offsets of derived $[\text{Fe}/\text{H}]$ of $\approx \pm 0.2$ dex can occur depending on how the measurement and calibration of the low resolution spectra is done. However, despite the difference in these estimates the robust implication is that the stars in Boo are both old and metal-poor.

In Fig. 1, we present new stellar iso-density contours based on deeper photometric data obtained with SuprimeCam mounted on the Subaru telescope. In contrast to the SDSS contours, the Subaru data suggest that Boo has a regular internal morphology, although some internal substructure may still be present (see Fig. 1). We note however, that some of the distortion seen in the inner contours is due to the presence of a very bright star in the field of view. It is thus possible that the internal morphology of Boo is quite regular. Both sets of contours exhibit elongation along an axis of roughly constant RA with an hint of an S-shape in the contours - we will use this later when choosing possible orbital paths for Boo.

3 SETUP

Based on the observed data discussed in § 1, there are four plausible assumptions which we can make in order to find possible orbits and progenitors of Boo:

(i) The iso-density contours of Boo are elongated approximately in the direction of constant RA and appear to show the (S-shaped) on-set of tidal tails. The tail-like features constrain the size of the luminous object and may be used to determine the projected orbital path.

(ii) The measured line-of-sight velocity dispersion is of order 7 km s^{-1} , which constrains the total mass of the object at the present epoch.

(iii) The scale-length (half-light radius) of the luminous matter is approximately $13'$ (corresponding to 230 pc at the distance of Boo) and the central surface brightness is of the order of $\mu_0 = 28 \text{ mag arcsec}^{-2}$.

(iv) The internal substructure seen in the contours of Fig. 1 is not real, but instead is likely to be an artifact of the sparse photometric data.

In choosing the properties of our Boo progenitors below, we will make use of some or all of these assumptions. We emphasise that these are assumptions for the present analysis, and their validity is amenable to future observational test.

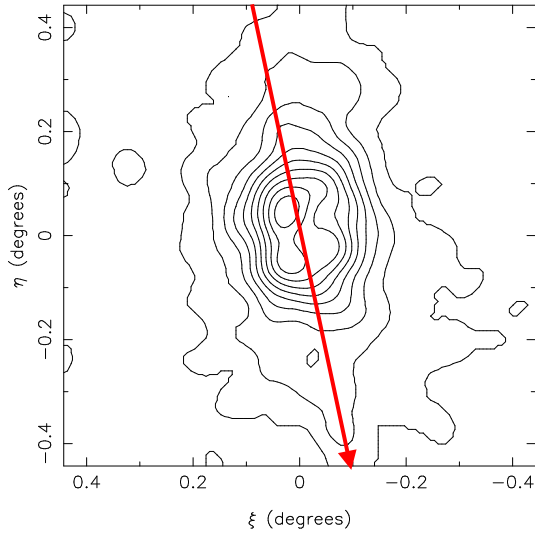


Figure 1. Contours of the Bootes dwarf satellite constructed from a stellar isopleth map of objects selected to occupy the main locus of Boo members in the CMD. Contours start at 2σ above the background in steps of 2σ . The photometric data were obtained using SuprimeCam mounted on the Subaru telescope. The straight (red) line shows a possible projected orbital path of Boo.

3.1 Galactic Potential

In our study, we model the Galactic potential analytically using a logarithmic halo of the form

$$\Phi_{\text{halo}} = \frac{1}{2}v_0^2 \ln(r^2 + d^2), \quad (8)$$

with $v_0 = 186 \text{ km s}^{-1}$ and $d = 12 \text{ kpc}$. Our choice of a spherical halo rather than a prolate or oblate model is motivated by our recent study of the tidal tails of the Sagittarius dSph, which showed that in the region probed by the debris from Sagittarius, the gravitational potential has to be close to spherical (Fellhauer et al. 2006). We model the disc as a Miyamoto-Nagai potential (Miyamoto & Nagai 1975) of the form

$$\Phi_{\text{disc}}(R, z) = -\frac{GM_d}{\sqrt{R^2 + (b + \sqrt{z^2 + c^2})^2}}, \quad (9)$$

with $M_d = 10^{11} M_\odot$, $b = 6.5 \text{ kpc}$ and $c = 0.26 \text{ kpc}$ (where R and z are cylindrical coordinates). The bulge is represented by a Hernquist (1990) potential

$$\Phi_{\text{bulge}}(r) = -\frac{GM_b}{r + a}, \quad (10)$$

using $M_b = 3.4 \times 10^{10} M_\odot$ and $a = 0.7 \text{ kpc}$.

3.2 Possible Orbits

As a starting point, we take the radial velocity of Boo at its present position to be $v_{\text{rad}} = 100 \text{ km s}^{-1}$ and its distance from the sun to be $D_\odot = 60 \text{ kpc}$. We use assumption (i) above to constrain the projected orbital path near the satellite. Furthermore, the shape of the stellar distribution near the on-set of the putative tidal tails suggests that the direction of motion along this path is likely to be from the top of Fig. 1 to the bottom. It is well-established that the tidal tails of a disturbed stellar system lie close to the orbital path of the system and that the leading arm should be closer to the

Table 1. The sample of the possible orbits of Boo simulated in this study. The first two columns give the proper motions of the orbit (the radial velocity at the present location of Boo is assumed to be 100 km s^{-1} in all cases). The third and fourth column give the peri- and apogalacticon distances and the last column gives the eccentricity of the orbit.

name	μ_α [mas yr $^{-1}$]	μ_δ [mas yr $^{-1}$]	R_{peri} [kpc]	R_{apo} [kpc]	e
(1)	-0.53	-0.62	1.8	66.2	0.95
(2)	-0.54	-0.70	4.7	66.2	0.87
(3)	-0.58	-0.90	14.8	67.2	0.64
(4)	-0.63	-1.20	36.9	76.7	0.35
(5)	-0.66	-1.40	48.8	104.3	0.36

Galactic Centre than the object while the trailing arm should be more distant (see e.g. Combes et al. 1999). In Fig. 1, the Galactic Centre lies approximately in the direction of the lower left corner of the figure which motivates our assumption regarding the direction of motion.

With the present-epoch radial velocity and projected path fixed, we use a simple point mass integrator to determine the forward and backward (in time) orbits for given pairs of assumed proper motions. Orbits which move along the assumed projected path are regarded as possible orbits of Boo. In Table 1 we give a selection of such orbits. They span a wide range of perigalactica, apogalactica and eccentricities and include orbits which have very close approaches to the Galactic Centre as well as orbits which spend most of their time in the outer Milky Way halo. Thus, despite restricting our models to the orbital path implied by assumption (i) we are still able to access the whole parameter space of possible eccentricities, peri- and apogalactic distances, even if assumption (i) turns out to be wrong.

We choose orbit (4) from Table 1 as the standard one for our simulations. This choice is more or less arbitrary and is justified only by the fact that it is not in any sense an extremal orbit: it neither gets very close to the Galactic Centre nor is it an orbit with a large apogalacticon. It also has a moderate eccentricity.

We also run models for orbit (3), which has an eccentricity more similar to the eccentricities of sub-halos seen in cosmological simulations (e.g. Ghigna et al. 1998) and one extreme model choosing orbit (2).

In our study, the simulation time is kept fixed at 10 Gyr. This choice is as arbitrary as the choice of orbit. It is likely that there is a trade-off between the choice of simulation time and the choice of orbit. For example, placing an object on an orbit with a close perigalacticon but only a short simulation time could lead to a similar remnant system as that produced by a progenitor farther out in the halo but whose evolution was followed for a longer time. However, while this would add another dimension to the (already vast) parameter-space of this problem, it would not affect our general conclusions about the properties of plausible progenitors.

3.3 Possible Progenitors

In order to determine the range of plausible progenitors for the satellite, we must now have a closer look at the properties of the Boo dwarf at the present epoch. If our assumption (i) regarding an interpretation of the morphology of the outer iso-density contours as the on-set of tidal tails is correct, this would imply an approximate tidal radius for Boo of about 250 pc. In our analytical model of the Milky Way, the enclosed mass (M_{MW}) at a distance

$D_{GC} \approx 60$ kpc is roughly $6 \times 10^{11} M_{\odot}$. Using the Jacobi limit for a satellite on a circular orbit (Binney & Tremaine 1987, their eq. 7-84):

$$r_{\text{tidal}} = \left(\frac{M_{\text{sat}}}{3M_{\text{MW}}} \right)^{\frac{1}{3}} D_{GC} \quad (11)$$

we find that the mass within the tidal radius of Boo is approximately $7 \times 10^4 M_{\odot}$, comparable to the observed luminous mass in Boo. While one should not over-interpret the closeness of the agreement given the crudeness of the above estimates, this suggests that it is possible to find progenitors for Boo which do not require that Boo be dark matter dominated. However, such models must also be consistent with the observed internal velocity dispersion, which provides tighter constraints. To illustrate this we now adopt a Plummer (1911) model for the satellite:

$$\rho_{\text{pl}}(r) = \frac{3M_{\text{pl}}}{4\pi R_{\text{pl}}^3} \left(1 + \frac{r^2}{R_{\text{pl}}^2} \right)^{-5/2} \quad (12)$$

with a Plummer radius (R_{pl} ; which corresponds to the half-light radius) of 200 pc. The formula

$$\sigma_{\text{los}}(0) \approx 2.52 \times \sqrt{\frac{M_{\text{sat}}[10^7 M_{\odot}]}{R_{\text{pl}}[\text{kpc}]}} [\text{km s}^{-1}] \quad (13)$$

yields a central line-of-sight velocity dispersion for such an object of only 0.5 km s^{-1} . This is in clear disagreement with the measured velocity dispersion of Boo.

With this background, we now explore the possibilities further. We first search for a dark matter-free (Plummer model) progenitor of Boo as our case A, to assess how well it can reproduce the observed morphology, keeping in mind our expectation that it will not be able to reproduce the observed velocity dispersion. In this model, the progenitor of Boo is similar to a 'star cluster' in the sense that it contains no dark matter, but it is unlike any known star cluster: its half-light radius is significantly larger than any observed star cluster. It resembles a dwarf galaxy like a tidal dwarf galaxy without dark matter content.

Alternatively, we can use Eq. 13 as a mass estimator and compute the mass of a model with a line-of-sight velocity dispersion of 7 km s^{-1} and a scale-length of 200 pc. This calculation yields a total mass of $1.5 \times 10^7 M_{\odot}$. Inserting this value into Eq. 11 we find that the tidal radius of Boo at its current location would be 1.2 kpc (or 1°). Although this is much larger than the apparent size of Boo, given the low surface brightness of the system it is possible that the stellar distribution extends significantly further than the contours of Fig. 1 might suggest. We therefore search for a possible progenitor using a single-component Plummer model as our case B, or mass-follows-light model. We note that if this model is correct, it would mean that the elongation of the stellar iso-density contours is intrinsic to Boo rather than being the on-set of tidal tails. We do not attempt to reproduce this elongation in our simulations, as this would add two more dimensions (angles of the initial orientation) to the space of free parameters in which we are searching for a progenitor, without changing our conclusions significantly. Although in this model the elongation is not tidally induced, we nevertheless use orbit (4) for this simulation to ease comparison with our 'star-cluster' model. As we discuss below, the results are qualitatively similar for a progenitor system placed on more extreme orbits. In a more general sense our model B could be regarded as a cored halo model with the luminous component having the same scale-length as the halo.

More fundamentally, there is no a priori reason why the stellar distribution should extend to the physical tidal radius. A simi-

lar argument applies to our models C1 and C2, in which we adopt a more elaborate, two-component representation of a dark matter-dominated satellite. We use a Hernquist (1990) profile:

$$\rho_{\text{H}}(r) = \frac{M_{\text{H}}}{2\pi} \frac{r_{\text{sc}}}{r} \frac{1}{(r + r_{\text{sc}})^3} \quad (14)$$

to represent the luminous matter (where M_{H} is the total luminous mass and r_{sc} is the scale-length) embedded in a halo of the form

$$\rho_{\text{NFW}}(r) = \rho_0 \frac{r_{\text{s}}}{r \left(1 + \frac{r}{r_{\text{s}}} \right)^2}, \quad (15)$$

(Navarro, Frenk & White 1996, henceforth NFW) where ρ_0 is the characteristic density and r_{s} is the scale-length. Due to the significant amount of mass at large radii in this model, such a progenitor will not develop tidal tails within the observed field of Boo. As in model B, therefore, this scenario requires the initial stellar distribution to be elongated. As before, we do not attempt to reproduce this elongation. We investigate two extreme sub-cases of scenario C (the extended DM scenario): first (C1) a luminous sphere embedded in a DM halo with the same scale-length and secondly (C2) a model with a very massive and extended DM halo whose scale-length is larger than the extent of the luminous matter. The parameters of both halos in our C models are broadly consistent with the outcome of large-scale cosmological Λ CDM simulations: in particular their scale radii and concentrations lie within the (broad) range expected for cosmological halos of these masses (Jing & Suto 2000).

In order to investigate further the possible relevance of putative tidal tails in dark matter-dominated models, we also consider a scenario in which the progenitor of Boo is on a quite extreme Galactocentric orbit. In this model, the satellite is initially deeply embedded in a much larger halo. To ensure that the luminous matter becomes tidally distorted, this system has to approach the Galactic Centre sufficiently closely that its tidal radius at perigalacticon shrinks to about 200 pc. To be consistent with the observed high velocity dispersion of Boo, the total mass of the object interior to this radius is $1.5 \times 10^7 M_{\odot}$. Using Eq. 11 and computing the enclosed mass of the Galaxy using the integrated forms of Eqs. 8–10 we see that in this case the perigalacticon of Boo's orbit must be about 5 kpc. During the perigalactic approach, the outer halo of Boo will become unbound and even the luminous part will be tidally shocked, developing tidal tails. As it moves to larger radii, the tidal radius expands to its much larger value at the present epoch and the residual outer halo, which did not have time to escape, becomes bound again. We call this our case D (or Dark Matter & tails model). For this model we use orbit (2) from Table 1.

Since our goal is a general analysis of possible histories of the Boo dSph galaxy, our parameter-space survey also included models in which the satellite is now in the final stages of disruption and dissolution. In order to be so strongly affected by tides, such models are necessarily of lower initial mass than the models which retain significant mass until late times. We found that such models could not reproduce the observed high velocity dispersion while simultaneously satisfying the constraint of the scale-length being 13 arcminutes (assumption iii). This conclusion holds using either single-component Plummer models or two-component, initially dark matter-dominated models as progenitors. That is, models which are not dark matter dominated but are tidally disrupting are not, in general, able to reproduce the observed velocity dispersion measured in Boo. This conclusion is of more general relevance for our understanding of the dark matter content of dSph galaxies.

This adds weight to our assumption that the internal photomet-

ric substructure in Boo is not real. While internal substructure is a possible signature of tidal disruption, it is rapidly erased in the interior of a massive, bound system (see e.g. Fellhauer & Kroupa 2005) except in certain circumstances (see e.g. Kleyna et al. 2003). The failure of disrupting models to reproduce the velocity dispersion of Boo suggests that the observed substructures are either kinematically very cold, or are due to noise in the photometric data set. It also means that the visible elongation of Boo is intrinsic to the progenitor of Boo and not tidally induced. Regarding the possible S-shape of the contours it can only be speculated that an initially flattened system, which is at least partly rotationally supported, might feel a tidally induced torque which bends the contours into an S-shape, even though the progenitor is deeply embedded in a DM halo (see e.g. Mayer et al. 2001). Given the current sparse nature of the observational data for Boo, such an investigation is not warranted in the context of the present paper.

We also investigated a more speculative scenario in which Boo had a recent encounter with the Sagittarius dwarf galaxy. In the absence of an observed proper motion, it is possible to find an orbit for Boo which would produce such a close passage around 340 Myr ago. The proper motion of Boo in this case would be $\mu_{\alpha \cos \delta} = +0.034 \text{ mas yr}^{-1}$, $\mu_{\delta} = -1.024 \text{ mas yr}^{-1}$. However, the remnant of Boo in this case is no more similar to the observed object than in the other scenarios we have considered and so the extra assumption of a two-body encounter with Sagittarius is not warranted.

For completeness, we also investigated a more exotic ansatz, namely ‘star cluster’ models (i.e. models without dark matter) which have a very massive black hole at their centre. As anticipated, even in the models which contained the most massive black hole which still led to an undisrupted object (in this case the central black hole was five times more massive than the stellar remnant) we could not reproduce the high velocity dispersion, even though the black hole-induced velocity dispersion dominated the bulk of the remnant.

3.4 Simulations

The modus operandi of our search for possible progenitors is the following:

- (i) We adopt a possible orbit for Boo. For most of our simulations this is our reference orbit (4) from Table 1.
- (ii) We use a simple point-mass integration to trace this orbit backwards for 10 Gyr.
- (iii) We insert the model for our possible progenitor at this starting position. In each model, each component of the model is represented by 10^6 particles.
- (iv) We simulate the model forward in time until the present epoch using the particle-mesh code Superbox (Fellhauer et al. 2000).
- (v) We analyse the final model and compare it to the observations. If there is a mismatch, we alter the initial properties of the progenitor (scale-length, mass, etc.) accordingly and start again with step (iii).

For all our models, we check for stability by evolving them first in isolation. The time evolution in isolation of the Lagrangian radii of some of our models are shown in Fig. 2. For the single-component Plummer models, the distribution function is used to generate the velocities. For the combined models we use the Jeans

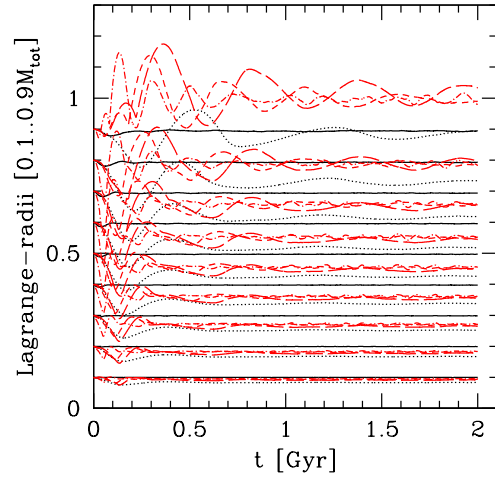


Figure 2. Lagrangian radii of our initial models evolved in isolation to demonstrate their stability. The plot shows the scaled Lagrangian radii (10%..90% of the total mass). The radii are scaled by their initial value and multiplied by the mass-fraction they represent. This results in initially equidistant radii independent of the choice of the initial profile, but also that the relative deviation of the 90% radius is displayed nine times larger than the deviation of the 10% radius. Dotted line is model A, solid line is model B, short dashed line is model C1, long dashed line is model C2 and dashed-dotted line represents model D. The additional models on orbit (3) are omitted for clarity. All models show an initial adaptation to the grid-based treatment. The additional luminous component for the models C1–D results in a slight contraction of the inner parts of the DM halo. Also an expansion of the outermost radius, due to the cut-off radius is visible. But after this short initial period the radii stay constant for the rest of the simulation time.

equation (see e.g. Binney & Tremaine 1987)

$$\sigma_{r,i}^2(r) = \frac{1}{\rho_i(r)} \int_r^{r_c} \frac{GM_{\text{tot}}(r')}{r'^2} \rho_i(r') dr', \quad (16)$$

and the Maxwellian approximation (e.g. Hernquist 1993) to generate the velocities. It is known (Kazantzidis, Magorrian & Moore 2004) that this approximation leads to a small core in the centre and a velocity anisotropy in the outer parts, i.e. enhancing the mass-loss of the outer shells. However, we note the addition of a luminous component to our models influences the DM distribution in the inner parts, making them more concentrated (Kazantzidis et al. 2004). This is clearly visible in Fig. 2 and below in Fig. 7. There we show that despite we use the Maxwellian approximation our DM haloes are cuspy in the centre and not cored even after 10 Gyr of evolution in a tidal field. A cored profile would indeed have a more impulsive response (due to the longer internal crossing time) to the tidal field and henceforth a larger mass-loss also in the inner parts, but we do not see this effect in our models. With regard to the incorrect treatment of the outer parts we note that we truncate our initial distribution at a radius which is only slightly larger than the tidal radius of Boo today, thereby reducing the initial mass-loss of the outer parts. A halo which extends to its virial radius (r_{200} , a quantity which is an order of magnitude larger than the tidal radius at first perigalacticon) would suffer strong mass-loss during its first peri-Galactic passage. Thus, the region from which we expect enhanced mass-loss due to the Maxwellian approximation would be removed by tides at early times. By starting with a smaller ini-

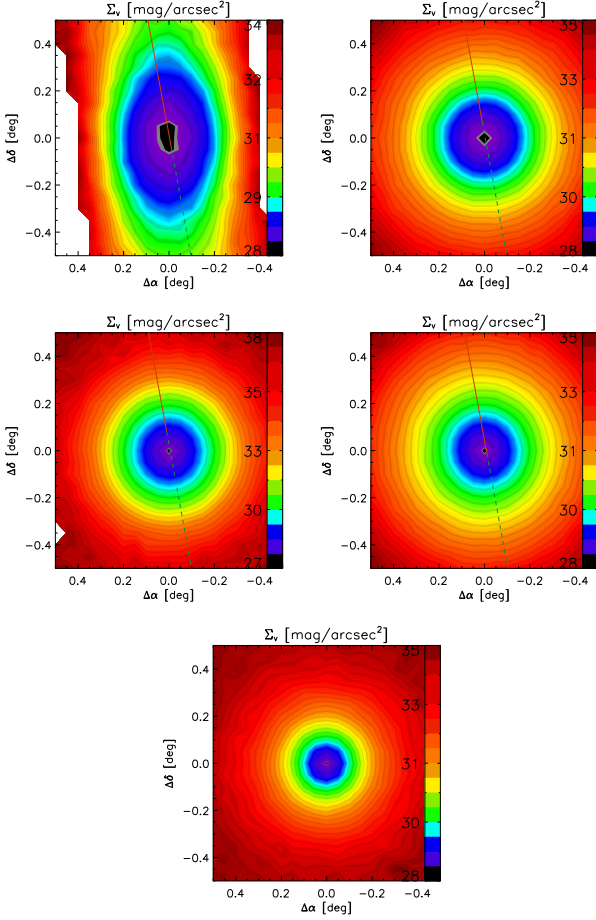


Figure 3. Surface brightness distribution of our models at the present epoch. **Top left:** case A, star cluster model; **top right:** case B, mass (stellar plus dark) follows light model; **middle left:** case C1, two-component, dark matter dominated model with halo of the same scale-length; **middle right:** case C2, 2-component, dark matter dominated with extended halo; **bottom:** case D, 2-component, dark matter dominated with tails. Models on orbit (3) are omitted.

tial truncation radius, we negate the impact of this mass loss on the evolution of our models.

4 RESULTS

In this section, we describe the best-fitting models of each type (A–D) introduced in §3.3. We show their initial parameters (relevant for the numerical setup) as well as the computed values of the virial radius, concentration and maximum circular velocity (relevant for comparison with other studies) in Table 2. The results of the Boo models at the present epoch, especially the inferred central mass-to-light ratios of Boo, are shown in Table 3.

4.1 The ‘star cluster’ case (A)

In this simulation we assume that the elongation of the outer stellar iso-density contours of Boo represents the on-set of tidal tails. This requires that the final model has a tidal radius of about 250 pc which, given the observed luminous mass, can only occur if the enclosed mass contains no dark matter contribution. We start with a

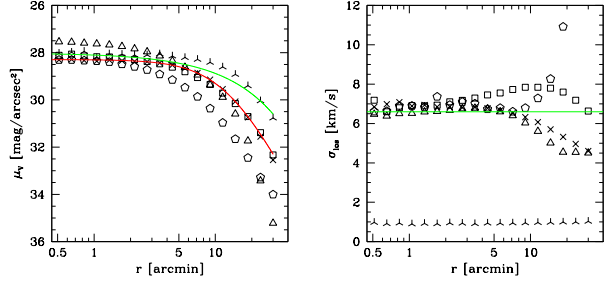


Figure 4. **Left:** Surface brightness profiles of our models. The upper (green) line shows the exponential fit to the observed data, while the lower (red) line shows the Plummer fit. **Right:** Velocity dispersion profiles of our models. The horizontal (green) line shows the observed value of the central velocity dispersion. The symbols are: Case A: tri-pods; case B: crosses; case C1: triangles; case C2: squares; case D: pentagons. Models on orbit (3) are omitted.

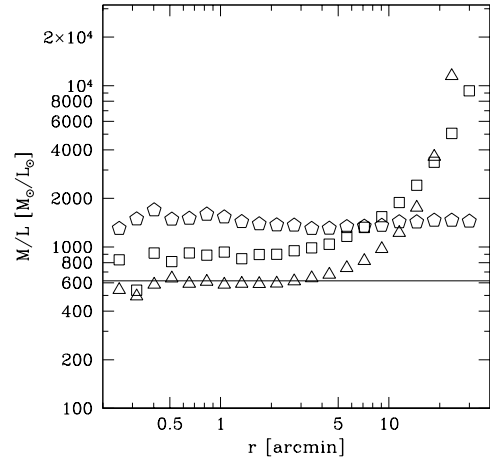


Figure 5. Radial variation of the mass-to-light ratios in our models. The horizontal line shows the constant value of case B (mass follows light). Triangles represent case C1, squares represent case C2 and pentagons are for case D. To convert the mass in luminous matter in our simulations to a luminosity for the stellar component we assume a mass-to-light ratio of two. Models of orbit (3) are omitted.

single Plummer sphere of mass $8 \times 10^5 M_\odot$ and Plummer radius (half-light radius) of 202 pc and truncate the distribution at 500 pc (see Table 2). We choose orbit (4) for this model because it fits the line-of-sight path traced by the tidal tails and is not extreme in any sense. The final object has a bound mass of $7.6 \times 10^4 M_\odot$ and a mass (including unbound material) of $1.1 \times 10^5 M_\odot$ lies within a field of view of one square degree. The object is strongly tidally distorted and elongated, although the iso-density contours remain quite smooth (see Fig. 3, top left panel). The radial surface density distribution reproduces the observed profile reasonably well (see Fig. 4 left panel) but the velocity dispersion of the final object is only of the order of 1 km s^{-1} (see Fig. 4 right panel). In fact, the remaining bound mass has an even lower dispersion ($\approx 0.5 \text{ km s}^{-1}$) but we observe an enhanced value in projection due to the unbound stars surrounding the object. The remnant exhibits no significant velocity gradients across the main body of the system. As expected, there is an offset of about 2 km s^{-1} , or roughly twice the internal

Table 2. Initial conditions for the best fitting models of all six cases. Shown are the basic parameters for each model and each component: initial mass, scale-length and cut-off radius. Furthermore we denote the virial radius ($r_{\text{vir}} = r_{200}$, except for the A-cases: $r_{\text{vir}} = -GM^2/4E$), the concentration $c = r_{\text{vir}}/r_s$, the mass at the virial radius, the maximum rotation velocity and finally the orbit (numbers refer to orbits in Table 1).

case	model	mass [M_\odot]	r_s [pc]	r_{cut} [pc]	r_{vir} [kpc]	c	$M(r_{\text{vir}})$ [M_\odot]	$v_{c,\text{max}}$ [km s^{-1}]	orbit
A	Plummer	8.0×10^5	202	500	0.34	1.7	5.1×10^5	4.1	(4)
B	Plummer	1.6×10^7	200	2000	1.4	7.0	1.6×10^7	18.5	(4)
C1	NFW	4.5×10^7	300	1200	12	40	1.5×10^8	13.1	(4)
	Hernq.	3.0×10^4	300	300					
C2	NFW	3.0×10^8	1000	2500	25	25	1.3×10^9	22.7	(4)
	Hernq.	4.0×10^4	250	500					
D	NFW	1.25×10^8	250	1000	18	72	5.1×10^8	23.9	(2)
	Hernq.	5.0×10^4	250	400					
A-3	Plummer	3.5×10^6	178	500	0.3	1.7	2.2×10^6	9.2	(3)
B-3	Plummer	2.0×10^7	200	1000	2.6	2.6	2.0×10^7	20.7	(3)
C1-3	NFW	5.0×10^7	300	1000	13	45	2.0×10^8	8.0	(3)
	Hernq.	5.0×10^4	300	500					
C2-3	NFW	6.0×10^8	1000	2500	32	32	2.8×10^9	61.0	(3)
	Hernq.	5.0×10^4	250	500					

Table 3. Parameters of the Boo models at the present epoch. The columns give the total mass within a field of view of one square degree ($\sim 1.1\text{kpc}$), the luminous mass within the field of view, the mean mass-to-light (M/L) ratio, the central mass-to-light ratio and the central velocity dispersion. For the simulation without dark matter the M/L-ratio quoted is in brackets and denotes the value which would be inferred by applying the virial theorem.

model	total mass [M_\odot]	lumin. mass [M_\odot]	$\overline{M/L}$	M/L_0	σ [km s^{-1}]
A	1.1×10^5	1.1×10^5	(17)	—	1.0
B	1.3×10^7	4.2×10^4	620	620	6.5
C1	2.7×10^7	3.0×10^4	1800	550	6.5
C2	6.7×10^7	3.9×10^4	3400	800	6.5
D	1.1×10^7	1.4×10^4	1400	1400	6.5
A-3	2.3×10^5	2.3×10^5	(32)	—	2.0
B-3	1.3×10^7	3.3×10^4	800	800	7.0
C1-3	1.1×10^7	2.9×10^4	740	600	5.5
C2-3	2.7×10^7	3.6×10^4	1500	1000	6.5

velocity dispersion, between the mean velocities of the leading and trailing tails.

Since this model can not reproduce the observed velocity dispersion of Boo, even when unbound stars along the line of sight are included, we conclude that a dark matter-free system is ruled out as a progenitor of Boo. Increasing the stellar mass of the progenitor would increase the velocity dispersion but would also reduce the level of tidal disturbance. As a result, the remnant would contain too much stellar mass and would not show evidence of tidal tails.

As a final possible avenue to obtain an inflated velocity dispersion (in projection) for a remnant without dark matter, we rotate the model (A) remnant so that the tidal tails lie along the line of sight. This configuration would be expected to maximise the observed velocity dispersion – Kroupa (1997) previously used such preferred alignments to argue that the dynamical masses of the larger dSphs were over-estimated. In the case of Boo, we note that its narrow

horizontal branch would argue against a significant line-of-sight extension in this system (see the colour magnitude diagram in Fig. 2 of Belokurov et al. 2006). Even given this optimal alignment, however, we find that the projected velocity dispersion of the remnant is smaller than 2 km s^{-1} . This adds further weight to our conclusion that all viable progenitors of Boo must have contained dark matter.

4.2 (Dark plus luminous) mass-follows-light: case (B)

This model is a simplified representation of a two-component progenitor with a cored luminous distribution together with a cored dark matter halo of the same scale-length and profile. In this scenario, the initial object is a Plummer sphere with a mass of $1.5 \times 10^7 M_\odot$. It has a Plummer radius of 200 pc and the distribution is truncated at 2 kpc (see also Table 2). At the present epoch, the remnant mass is about $1.3 \times 10^7 M_\odot$, a value which agrees closely with our simple mass estimate from § 3.3. The central line-of-sight velocity dispersion is 6.5 km s^{-1} which agrees with the observed value and the final scale-length is 13 arcsec as observed. To reproduce the radial surface-brightness profile and the total luminous mass, a mass-to-light ratio of 620 is required (see Fig. 3 top right panel). The resulting surface brightness and velocity dispersion profiles are shown as crosses in Fig. 4. The surface brightness profile is very close to the observed Plummer fit to the profile of Boo, which is unsurprising given that the inner regions of this model are shielded from the effects of tides. We note, however, that at larger radii (not visible in the field of view shown in Fig. 3) this model exhibits the on-set of tidal tails.

One might also speculate that the dark matter halo of Boo’s progenitor was cored but with a scale-length much larger than that of the light. In such a model, dark matter at large radii would be tidally stripped at earlier times. As a result, the scale-lengths of the dark and luminous matter distributions would become more similar over time, leading to a model which was closer to mass-follows-light at the present epoch. We therefore conclude that a cored halo model is a plausible progenitor for Boo and, further, that a total

mass-follows-light model is consistent with the currently available data.

As we discussed earlier, this model does not reproduce the elongation of Boo but remains spherical, having the same luminous mass and scale-length as the observations. Since the inner regions of this model (corresponding to the volume probed by the observed stellar distribution) are almost unaffected by the external tidal field, we expect that our results would change only marginally if we used an elongated model with the same mass and mean scale-length at the start of the simulation. However, although this would not strengthen our conclusions regarding the viability of this scenario, it would greatly increase the computational effort required to identify suitable progenitors as we would have to constrain two additional free parameters (orientation angles) unrelated to the important physical structure of Boo in order to match the observed orientation of Boo.

Both model A and model B compare well with Johnston, Choi & Guhathakurta (2002), probing just much smaller scales, even though in model B features like isophotal twist and the break radius are beyond the field of view of Fig. 3 and 4. It is the 'diffuse light' around model A which boosts its 'measured' velocity dispersion by a factor of two.

4.3 Extended dark matter: case (C)

C1: In this simulation, the dark matter halo and the luminous matter have the same scale-length but differing initial radial structure and radial extent (see Table 2). In order to match the high central velocity dispersion, this model requires a concentrated halo, with a correspondingly low total mass. As a result, halo material can be easily stripped from the outer parts of the system. At the present epoch in our simulation we find $3 \times 10^4 M_\odot$ of luminous matter in the field of view (see Fig. 3 middle left panel) and $2.7 \times 10^7 M_\odot$ in dark matter, which agrees approximately with our estimate from Section 3.3. The average M/L-ratio within one square degree is 1800. If we analyse the radial dependence of the M/L-ratio (see Fig. 5) we see that in the very centre the value is about 550 and therefore similar to our mass follows light case (B) and it increases only in the very outer parts where virtually no stars are present. At the present epoch in the simulations the stellar distribution is slightly elongated at larger radii (outside our field of view) although we started with a perfectly spherical distribution. This shows that a lot of dark matter in the outer parts has been stripped away, and the outer luminous part of the satellite is feeling the tidal forces of the Milky Way. The final radial surface brightness profile is similar to that of Boo, although the central value is slightly higher. As with model (B), the elongation of the satellite at radii less than 0.5° is not reproduced - an initially flattened progenitor would probably yield a remnant with a density distribution more similar to that of Boo. The velocity dispersion within $10'$ matches the observed value, although it falls off at larger radii.

C2: In this scenario, we have an initial model where the luminous matter is represented by a Hernquist sphere embedded in a significantly more extended NFW halo. The initial scale-length of the halo is larger than the initial size of the luminous distribution (see Table 2). This model reproduces the high velocity dispersion of Boo but extends to much larger radii than the observed object. By the end of simulation, we find $3.9 \times 10^4 M_\odot$ of luminous matter within one square degree but $6.7 \times 10^7 M_\odot$ of DM. These values imply a mean M/L-ratio of more than 3400, which would be

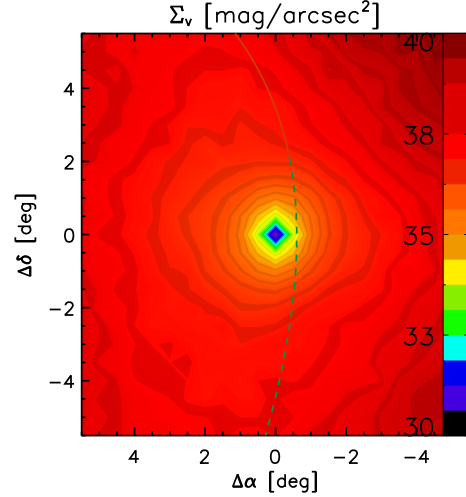


Figure 6. Surface brightness distribution over a larger area, complementary to Figure 2, for model (D) in which the progenitor is on an extreme orbit about the Milky Way.

the highest claimed ratio within the region probed by the stars in any Milky Way satellite so far, but are comparable to those derived in NFW-based modelling by Penarrubia, Navarro & McConachie (2007). As Fig. 5 shows, in the innermost regions the M/L-ratio of this model is about 800 but it increases exponentially with radius up to a value of ≈ 9000 .

Due to its massive, extended halo, this model has no tidal tails inside the optical radius. However, the surface brightness profile closely matches the observed profile (see Fig. 4), and the high central velocity dispersion is also reproduced. As in the previous models, we do not account for any initial ellipticity of Boo.

We conclude that if we were to allow some intrinsic elongation either of our NFW halo scenarios could account for the observed properties of Boo.

4.4 Dark matter & tails: case (D)

In this model we attempt to retain the assumption that the observed elongation of Boo is the onset of tidal tails in a dark matter-dominated model. Therefore, we place the progenitor on a more eccentric orbit. For this scenario to be viable, the perigalacticon of the orbit must be sufficiently close to the Galactic Centre that the tidal radius of Boo shrinks to a value such that even the deeply-embedded luminous matter is affected by the external field. In fact, we find that the simulation does not show tidal distortion on small scales, although some hint of tails are noticeable on larger scales (see Fig. 6). As in our other dark matter-dominated models, the velocity dispersion of Boo is reproduced. However, the evolution leads to a surface brightness profile which falls off somewhat more steeply than the observed profile. In the field of view, we find $1.4 \times 10^4 M_\odot$ in stars and $10^7 M_\odot$ in DM, giving an average M/L-ratio of about 1400. As Fig. 5 shows, the M/L-ratio is roughly constant throughout the remnant.

This simulation shows that even though the tidal radius at perigalacticon shrinks to values well within the luminous distribution, and some stars become unbound, the resulting stellar remnant does not exhibit tidal tails at the present epoch. During the long period of the orbit where the tidal radius is much larger than the extent of the

luminous matter, formerly unbound stars become bound again and, apparently, redistribute themselves symmetrically about the remnant due to phase mixing. Given the absence of tails, we conclude that this model is no more successful in reproducing the observations than our other dark matter-dominated models and merely serves to illustrate that our conclusions relating to models (B), (C1) and (C2) would be largely unchanged if those progenitors were placed on more extreme orbits.

4.5 Orbit (3) models

Because neither orbit (4) nor the extreme orbit (2) are based on cosmological assumptions we also perform a suite of simulations using orbit (3), which is more typical of the range of eccentricities found in cosmological simulations. We search for initial models for our four orbit (4) cases, namely A to C2 and compare the different models. The initial conditions and the final results are shown in Table 2 and Table 3 respectively. Comparing the initial values, there is a clear trend that the initial masses have to be higher to reproduce the same kind of remnant today. One can also notice the trend that the final models have larger central mass-to-light ratios than their corresponding models on orbit (4). This trend is best visible if one compares the sequence of the models C1(-4), C1-3 and D (or C1-2). The initial mass increases with decreasing perigalacticon and also the final central mass-to-light ratio increases from 550 via 600 to an astonishing value of 1400 in the most extreme case.

To simplify the comparison between our models, we kept the same initial scale-lengths from our orbit (4) models in our DM-dominated simulations for progenitors on orbit (3). In order to shield the luminous component from tidal disruption, we then have to make the orbit (3) models more massive. As a result, the initial central M/L-ratios were higher in the orbit (3) models as well as the central velocity dispersions. However, the halos on orbit (3) are tidally shaped differently, because they experience a stronger tidal field and therefore at the end of the simulation the halo scale-lengths in our orbit (3) models differ from the ones on orbit (4). Due to this fact, we still see higher central values for the M/L-ratio although the final velocity dispersions are similar.

In our heavily dark matter-dominated simulations we find only a slight evolution of the luminous component with time. But the halo component experiences a rather strong tidal shaping in its outer parts. We show the time evolution of the halo density profile of one of our models (C1-3) in Fig. 7. Still our model of the DM halo shows a cuspy profile even after 10 Gyr of evolution, i.e. the influence of the tides on the innermost parts of the satellite is rather weak. Due to the interplay of dark and luminous component effects as discussed in Kazantzidis, Magorrian & Moore (2004) seem not to play a strong role in our simulations.

5 CONCLUSIONS

In this paper we have investigated a wide range of possible progenitors and evolutionary histories for the recently discovered Bootes dwarf spheroidal satellite galaxy of the Milky Way. As we discussed in § 3.3, although the outer iso-density contours of the stellar distribution are elongated, an observation sometimes interpreted as suggestive of tidal disturbance, this interpretation is not consistent with the observed velocity dispersion of $\approx 7 \text{ km s}^{-1}$. Our initial attempts to reproduce both the distorted outer morphology and high velocity dispersion using models which were close to, or slightly beyond, the point of complete disruption were unsuccessful. We

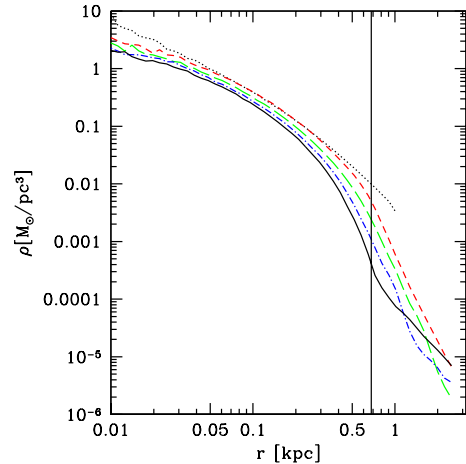


Figure 7. Evolution of the density profile of model C1-3. Shown are the initial profile (dotted, black), at $t = 2.5$ Gyr (short dashed, red), at that time the satellite is near its perigalacticon, at $t = 5$ Gyr (long dashed, green), at $t = 7.5$ Gyr (dashed-dotted, blue) close to its apogalacticon and the final profile at $t = 10$ Gyr (solid, black). Vertical line denotes the tidal radius at perigalacticon.

therefore focused on bound models either with or without the presence of significant quantities of dark matter.

Our model (A) is an extended 'star cluster' model and reproduces the surface brightness profile and distorted outer morphology of Boo reasonably well. As expected for a purely stellar system from our argument in § 3.3, however, the final velocity dispersion is significantly smaller than that observed in Boo. It is therefore very unlikely that a purely stellar model could be the origin of Boo.

Our dark matter-dominated models (cases (B) - (D)) can reproduce both the surface brightness profile and the velocity dispersion, but not the morphology of the outer stellar distribution. This morphological limitation is because all our progenitors are initially spherical, and their dark matter halos protect them from significant tidal disturbance. Even if the orbit of Boo has a very small perigalacticon (case (D)), the remnant does not exhibit tidal tails on scales as small as those observed in Boo. For these models therefore, if the elongation of the outer contours of Boo is real and not an artifact of the sparse photometric data, then it must result from intrinsic elongation of the progenitor system. As stated in § 3.3 the putative S-shape of the contours in these cases do not represent the on-set of tidal tails but might be caused by tidal torques acting on an intrinsically flattened system which is at least partly rotationally supported but remains deeply embedded in its DM halo. Given the very low stellar mass of a faint satellite like Boo, a dwarf disc galaxy progenitor (such as was used by Mayer et al. (2002) to model the Carina dSph) would either have to be orders of magnitude lower in baryonic mass than typically observed stellar discs, or would have to lose almost all of its initial mass (both dark and baryonic). The latter scenario would either require an extremely low star formation efficiency in the original disk (i.e. most of the baryonic component is still in the form of gas, which gets easily stripped by ram pressure stripping and the cosmic ultraviolet background at high redshift as suggested by Mayer et al. (2007)), or very strong tidal disturbance. Again we emphasise that to reproduce the high velocity dispersion of Boo, we require a dark matter mass in the inner regions which would preclude this level of tidally-induced

mass loss from the central parts - in our study it was not possible to reproduce the data of Boo with a disrupted object of any kind.

On the basis of our study, we conclude that it is unlikely that the progenitor of Boo contained no dark matter. In fact, we found no viable models in which dark matter was not always dominant. External tidal effects on the evolution of the progenitor of Boo do not significantly affect the observed stellar velocity dispersion in the inner regions, or the structure of the galaxy. Our most likely models have final DM masses in the range $1 - 7 \times 10^7 M_\odot$.

By changing the possible orbit of Boo we found that the closer the orbit gets to the Galactic centre (i.e. smaller perigalacticon and higher eccentricity) the larger is the mass-to-light ratio exhibited in the undisturbed central part of the final model.

In order to understand properly the details of the specific Bootes galaxy progenitor, however, further data are required. First, deeper photometric data extending to larger radii around the satellite are essential in order to establish the full extent of the remnant and whether there is any evidence that the elongation is tidal in origin (e.g. whether the elongation links to larger scale tidal arms). Secondly, a larger kinematic data set is required to study the variation of the velocity dispersion and mean velocity with position in Boo. This would yield further information about the mass distribution within the remnant. Both these studies are currently underway.

Acknowledgements: MF, VB and DBZ acknowledge funding by STFC. MIW acknowledges support from a Royal Society University Research Fellowship. We thank Rainer Spurzem and Walter Dehnen for useful comments.

REFERENCES

- Aaronson M., 1983, *ApJ*, 266, L11
 Bailin J., Ford A., 2007, *MNRAS*, 375, L41
 Battaglia G., Irwin M., Tolstoy E., Hill V., Helmi A., Letarte B., Jablonka P., 2007, *MNRAS* accepted, arXiv:0710.0798
 Belokurov V., et al., 2006a, *ApJ*, 647, L111
 Belokurov V., et al., 2007, *ApJ*, 654, 897
 Binney J., Tremaine S., 1987, 'Galactic Dynamics', Princeton Series in Astrophysics, Princeton University Press
 Combes F., Leon S., Meylan G., 1999, *A&A*, 352, 149
 Fellhauer M., Kroupa P., Baumgardt H., Bien R., Boily C.M., Spurzem R., Wassmer N., 2000, *NewA*, 5, 305
 Fellhauer M., Kroupa P., 2005, *MNRAS*, 359, 223
 Fellhauer M., et al., 2006, *ApJ*, 651, 167
 Ghigna S., Moore B., Governato F., Lake G., Quinn T., Stadel J., 1998, *MNRAS*, 300, 146
 Gilmore G., Wilkinson M.I., Wyse R.F.G., Kleya J.T., Koch A., Evans, N.W., 2007, *ApJ*, 663, 948
 Hernquist, L., 1990, *ApJ*, 356, 359
 Hernquist, L., 1993, *ApJS*, 86, 389
 Jing Y.P., Suto Y., 2000, *ApJ*, 529, L69
 Johnston K.V., Sigurdsson S., Hernquist L., 1999, *MNRAS*, 302, 771
 Johnston K.V., Choi P.I., Guhathakurta P., 2002, *AJ*, 124, 127
 Kazantzidis S., Kravtsov A.V., Zentner A.R., Allgood B., Nagai D., Moore B., 2004, *ApJ*, 611, L73
 Kazantzidis S., Magorrian J., Moore B., 2004, *ApJ*, 601, 37
 King I., 1966, *AJ*, 71, 61
 Kleya J.T., Wilkinson M.I., Evans N.W., Gilmore G., 2001, *ApJ*, 563, L115
 Kleya J.T., Wilkinson M.I., Gilmore G., Evans N.W., 2003, *ApJ*, 588, L21
 Koch A., Kleya J.T., Wilkinson M.I., Grebel E.K., Gilmore G., Evans N.W., Wyse R.F.G., Harbeck D.R., 2007, *AJ*, 134, 566
 Kroupa P., 1997, *New Astronomy*, 2, 139
 Martin N.F., Ibata R.A., Chapman S.C., Irwin M.J., Lewis G.F., 2007, *MNRAS*, 380, 281
 Mateo M., 1998, *ARA&A*, 36, 436
 Mayer L., Governato F., Colpi M., Moore B., Quinn T., Wadsley J., Stadel J., Lake G., 2001, *ApJ*, 559, 754
 Mayer L., Moore B., Quinn T., Governato F., Stadel J., 2002, *MNRAS*, 336, 119
 Mayer L., Kazantidis S., Mastropietro C., Wadsley J., 2007, *Nature*, 445, 738
 Miyamoto M., Nagai R., 1975, *PASJ*, 27, 533
 Moore B., Ghigna S., Governato F., Lake G., Quinn T., Stadel J., Tozzi P., 1999, *ApJ*, 524, L19
 Muñoz R.R., Carlin J.L., Frinchaboy P.M., Nidever D.L., Majewski S.R., Patterson R.J., 2006, *ApJ*, 650, L51
 Navarro J.F., Frenk C.S., White S.D.M., 1996, *ApJ*, 490, 493
 Penarrubia J., Navarro J.F., McConachie A.W., 2007, *ApJ*, accepted (arXiv:0708.3087)
 Plummer H.C., 1911, *MNRAS*, 71, 460
 Read J. I., Wilkinson M. I., Evans N. W., Gilmore G., Kleya J. T., 2006, *MNRAS*, 367, 387
 Rutledge G.A., Hesser J.E., Stetson P.B., 1997, *PASP*, 109, 907
 Siegel M.H., 2006, *ApJ*, 649, L83
 Walsh S.M., Jerjen H., Willman B., 2007, *ApJ*, 662, L83
 Willman B., et al., 2005, *ApJ*, 626, L85
 York D.G., et al., 2000, *AJ*, 120, 1579
 Zucker D.B., et al., 2006, *ApJ*, 650, L41